Int. J. Electrochem. Sci., 14 **(2019)** 1358 – 1371, doi: 10.20964/2019.02.51

International Journal of
ELECTROCHEMICAL
SCIENCE
www.electrochemsci.org

Assembly Mechanics and Its Effect on Performance of Proton Exchange Membrane Fuel Cell

Guilin Hu [1,2,], Chen Ji[1], Yuzhen Xia[1], Yange Suo[1], Xiaojun Wu[1], Zhiguo Zhang[1]*

[1] Department of Energy and Environment System Engineering, Zhejiang University of Science and Technology, Hangzhou, 310023, P. R. China
[2] Department of Chemical and Biological Engineering, University of British Columbia, 2360 East Mall, Vancouver B.C. V6T 1Z3, Canada
[*]E-mail: enehgl@163.com

Received: 12 October 2018 / *Accepted:* 15 November 2018 / *Published:* 5 January 2019

The safe operation and satisfactory cell performance of a proton exchange membrane fuel cell (PEMFC) depend on suitable assembly pressure. In order to obtain this, different assembly pressures and their effect on cell performance are investigated. The numerical simulation was employed to study the gas diffusion layer (GDL) deformation under different assembly pressures. The effect of assembly pressure on transportation parameters such as GDL porosity and permeability, and final influence on the performance of PEMFC, was studied to obtain optimal assembly pressure. The geometrical model of a single PEMFC channel was established. Parameters such as porosity and permeability of the GDL under different assembly pressures were calculated according to an empirical formula. Finite element analysis (FEA) was used to analyze the effect of different assembly pressures on GDL deformation. The results show that the GDL part under the bipolar plate ribs is deformed to different degrees under the compression of assembly pressure, and the degree of deformation increases as the assembly pressure increases, while the GDL part under the channel is almost not deformed. The distribution of the reactant species concentration in the single PEMFC channel and the polarization curves under different assembly pressures were computed and compared. Reactant species concentrations decrease in the flow direction under all assembly pressures for reaction in the catalyst layer. It is seen from the polarization curves that a fuel cell under an assembly pressure of between 0.5 and 1.0 MPa performs best.

Keywords: proton exchange membrane fuel cell (PEMFC), assembly mechanics, numerical simulation, gas diffusion layer (GDL), porosity

1. INTRODUCTION

A PEMFC has many advantageous characteristics, especially low or zero emission, short startup time and gas filling time, which make it a promising candidate as power source of future transport vehicles such as fuel cell cars. In order to deeply investigate the transportation phenomena, there are lots

of researches involving the mathematical modeling and numerical simulation of PEMFC [1-6]. All the components of PEMFCs need to be assembled together suitably for good species transportation and low electrical resistance. The GDL is a porous structure and its modulus of elasticity is relatively small. If the assembly pressure is too high, it will cause over-deformation or even irreversible damage to the GDL, thus narrowing the gas transportation channel, increasing mass transfer resistance, and even damaging the fuel cell components and so shorting the fuel cell's life. Sometime the big assembly pressure will produce plastic deformation or cracking for stresses in some stack components 1. Reversely, if the assembly pressure is too low, contact electrical resistance will increase due to poor contact between the GDL and the bipolar plate. This will reduce fuel cell efficiency, and increase the risk of reactant gases leaking. Thus, the optimal clamping load and displacement should be studied to obtain good cell performance 8.

The effect of assembly clamping pressure on the GDL and the performance of PEMFCs was studied by Xing et al. 9 using the simultaneous perturbation stochastic algorithm method, the optimum clamping pressures under different operating voltages was obtained. Lee et al. 10 calculated the pressure distribution in the single cell using the finite element analysis (FEA) procedures. The calculated results were verified by experiments. A pressure film was inserted between the bipolar plates and the membrane electrode assembly (MEA) to test the pressure distribution. Mason et al. 11 investigated relationship between GDL thickness and contact resistance under different compaction pressure using an in-situ analytical technique based on simultaneous displacement and resistance measurement of GDLs in PEMFCs. Yim et al. 12 investigated the effect of GDL compression on fuel cell performance using a 5-cell PEMFC stack with GDL compressions 15% and 30%. Results showed that the PEMFC stack with high GDL compression (30%) have better performance than low GDL compression (15%) at all current ranges, which means that the decrease in contact resistance at higher GDL compression has a greater effect on stack performance than does the increase in mass transport resistance. Taymaz et al. 13 computed fluid flow, electrochemical reactions and the effect of assembly pressure on fuel cell performance using a three-dimensional computational fluid dynamics (CFD) fuel cell model, which is based on a deformed geometrical model obtained by a finite element analysis (FEA) model for single PEMFC. Zhou et al. 14 calculated mechanical deformation, mass transfer resistance, and electrical contact resistance simultaneously based on a finite-element mass-transfer and structural model. Furthermore, Zhou et al. 15 developed a new model to investigate the effect of assembly pressures, temperatures, and humidity on stack mechanical behavior. Gas flow, diffusion and chemical reactions were determined based on the deformed geometrical model and updated material properties. Further developing previous model, zhou et al. [16] conducts a comprehensive research about the effects of assembly pressure, operating temperature and humidity on PEM fuel cell stack deformation, contact resistance and overall performance. The thermal stress distributions in a high-temperature proton exchange membrane fuel cell (HT-PEMFC) were numerically examined by Oh [17]. The stress-temperature interaction during HT-PEMFC operations was obtained by numerical simulation; the coupled FEM/CFD HT-PEMFC model can be used as a useful tool for optimizing HT-PEMFC contact compression and other operating conditions. The effects of GDL compression/intrusion on the performance of a HT-PEMFC was numerically investigated by a combined FEM/ CFD methodology [18]. Three-dimensional FEM simulations were conducted to analyze cell GDL deformation under

various displacement clamping conditions. Then, transport and electrochemical processes during HT-PEMFC operation was studied using a multidimensional HT-PEMFC CFD model. A two-dimensional study was conducted using CFD with an idealized fibrous medium representing the GDL of a PEMFC [19]. The relationship between the compression ratio and the permeability of the medium were deduced and key parameters governing the changes in flow were determined. Results show that compression reduces the absolute permeability of an isotropic medium. Finite element analysis using ANSYS was conducted to learn the stress and deformation during assembly [20]. The effect of clamping loads was investigated for different forces and for different displacements, and the appropriate load and displacement are obtained for single cell assembly.

Hitherto, the coupled stress-strain and CFD model and simulation is seldom seen in public publication. The effect of compression on transportation phenomena and the performance of PEMFCs are investigated in this paper. A geometrical model of a PEMFC after compression was obtained and subjected to further simulation using FLUENT to estimate performance. The compression effect of different assembly pressures are then computed and compared and an optimum assembly pressure is subsequently determined for the actual fuel cell assembly.

2. MATHEMATICAL AND PHYSICAL MODELS

2.1 Model assumptions

In order to simplify the simulation, the following assumptions were made:

(a) All deformation is elastic and homogenous. The simulation results justify this——the simulated maximum equivalent stress was a small fraction of the yield strength of the PEMFC materials.

(b) The reactants do not permeate through the proton exchange membrane.

(c) The material properties are independent of temperature.

(d) All materials are isotropic and homogenous.

(e) The system is considered as steady-state.

2.2 Geometrical model

Generally, a PEMFC is composed of nine segments, as illustrated in figure 1 [5]: current collectors, gas channels, gas diffusion layers and catalyst layers on both the anode and the cathode sides, and a proton exchange membrane in the middle. The outer current collectors are carved with flow channels to allow reactants to enter and products to exit the cell. The porous backing layers provide even distribution of reactants to the anode and cathode catalyst layers. The central polymer membrane physically divides the fuel cell into anode and cathode. The function of membrane not only avoids reactant species and electron passing directly through the cell, but provides a pathway for proton. The catalyst layers are a core domain for electrochemical reactions, which provide electron, proton and reactant channels. In order to reduce the computation resources and computation time required, we take one single channel and corresponding components as computation domain, as shown in figure **1**.

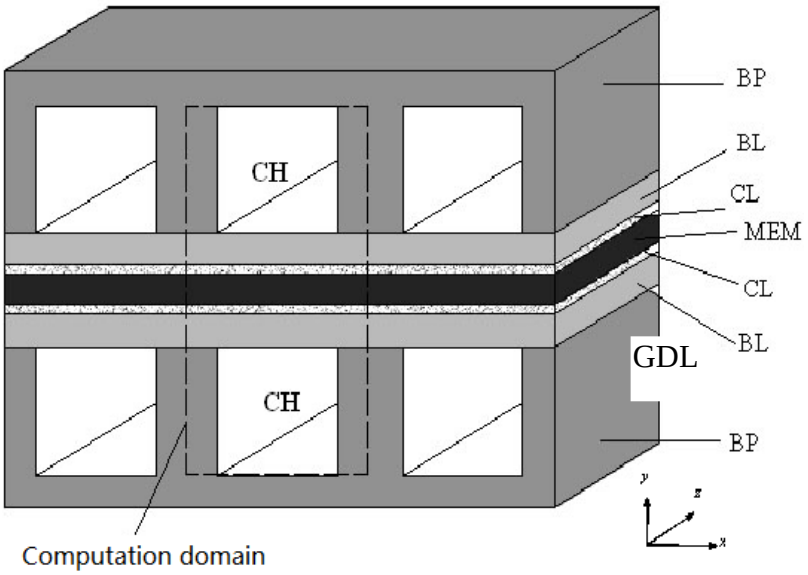

Figure 1. Schematic of computation domain (BP-bipolar plate; GDL -Gas diffusion layer; CL-catalyst layer; MEM-membrane) [5]

2.3 Equations governing transportation phenomena inside the fuel cell

Numerical simulation is based on a three-dimension, multi-component, non-isothermal, comprehensive model considering deformed geometry, which includes mass, momentum, energy and reactant species transportation. So the general equation of continuum, momentum, species conservation and energy conservation are described as follows [6]:

$$\nabla \cdot (\varepsilon \rho \boldsymbol{u}) = S_{\mathrm{m}} \tag{1}$$

$$\nabla \cdot (\varepsilon \rho \boldsymbol{u}.\boldsymbol{u}) = -\varepsilon \nabla p + \nabla \cdot (\varepsilon \mu^{\mathrm{eff}} \nabla \boldsymbol{u}) + S_{\boldsymbol{u}} \tag{2}$$

$$\nabla \cdot (\varepsilon \rho \boldsymbol{u} C_i) = \nabla \cdot (-\rho D_i^{\mathrm{eff}} \nabla C_i) + S_i \tag{3}$$

$$\nabla \cdot (\rho \boldsymbol{u} C_p T) = \nabla \cdot (\lambda^{\mathrm{eff}} \nabla T) + S_T \tag{4}$$

Where ε is porosity of media, ρ is mixture density, $\boldsymbol{u}$ is intrisinic fluid velocity, S_{m} is mass source term, p is fluid pressure, μ^{eff} is effective viscous coefficient, $S_{\boldsymbol{u}}$ is movement source term, C_i is mass fraction of species i, S_i is mass source term of species i, T is temperature, C_p is iso-pressure heat capacity, λ^{eff} is effective heat conductivity, S_T is energy source term. The mass source term S_i of species produced by electrochemical reaction in the catalyst layer, can be determined by

$$S_i = \frac{r}{nF} j \tag{5}$$

where F is Faraday's constant, n is number of transfer electron for ith species, r is stoichiometric number, j is transfer current density. Thus, the mass source terms for the reacting species hydrogen, oxygen and water become

$$S_i = \begin{cases} -\dfrac{j_a}{2F} & \text{for } H_2 \\ \dfrac{j_c}{4F} & \text{for } O_2 \\ -\dfrac{j_c}{2F} & \text{for } H_2O \end{cases} \tag{6}$$

2.4 Theoretical stress-strain model

In order to calculate the deformation of the GDL, the equations expressing the relationship between stress, strain and external load forces can be written thus:

（1）the force balance equations：

$$\begin{cases} \dfrac{\partial \sigma_x}{\partial x} + \dfrac{\partial \tau_{yx}}{\partial y} + \dfrac{\partial \tau_{zx}}{\partial z} + X = 0, \\ \dfrac{\partial \sigma_y}{\partial y} + \dfrac{\partial \tau_{zy}}{\partial z} + \dfrac{\partial \tau_{xy}}{\partial x} + Y = 0, \\ \dfrac{\partial \sigma_z}{\partial z} + \dfrac{\partial \tau_{xz}}{\partial x} + \dfrac{\partial \tau_{yz}}{\partial y} + Z = 0, \end{cases} \tag{7}$$

Where σ_x, σ_y, σ_z are the positive stresses in the *x, y* and *z* directions; X, Y, Z are body forces in the corresponding directions. τ_{xy} , τ_{yz} and τ_{zx} are shear stresses, which have the following relationship:

$$\begin{cases} \tau_{xy} = \tau_{yx}, \\ \tau_{yz} = \tau_{zy}, \\ \tau_{zx} = \tau_{xz}, \end{cases} \tag{8}$$

（2）deformation geometry equations:

$$\begin{cases} \varepsilon_x = \dfrac{\partial u}{\partial x}, \quad \varepsilon_{xy} = \dfrac{1}{2}\left(\dfrac{\partial u}{\partial y} + \dfrac{\partial v}{\partial x}\right), \\ \varepsilon_y = \dfrac{\partial v}{\partial y}, \quad \varepsilon_{yz} = \dfrac{1}{2}\left(\dfrac{\partial v}{\partial z} + \dfrac{\partial w}{\partial y}\right), \\ \varepsilon_z = \dfrac{\partial w}{\partial z}, \quad \varepsilon_{zx} = \dfrac{1}{2}\left(\dfrac{\partial w}{\partial x} + \dfrac{\partial u}{\partial z}\right), \end{cases} \tag{9}$$

Where ε_x, ε_y and ε_z are positive strain in different directions; ε_{xy} 、 ε_{yz} 、 ε_{zx} are shear strains; u 、 v 、 w are displacements in *x, y, z* directions.

（3） the physical stress-strain equation:

$$\begin{cases} \varepsilon_x = \dfrac{1}{E}\left[\sigma_x - \mu(\sigma_y + \sigma_z)\right], \\ \varepsilon_y = \dfrac{1}{E}\left[\sigma_y - \mu(\sigma_z + \sigma_x)\right], \\ \varepsilon_z = \dfrac{1}{E}\left[\sigma_z - \mu(\sigma_x + \sigma_y)\right], \end{cases} \tag{10}$$

Where E is the modulus of elasticity, and μ is Poisson's ratio. When the total elastics is homogeneous, the physical equation can be represented as Hooke's law, so the shear strain and shear stress can be related as follows:

$$\begin{cases} \gamma_{xy} = \dfrac{\tau_{xy}}{G}, \\ \gamma_{yz} = \dfrac{\tau_{yz}}{G}, \\ \gamma_{zx} = \dfrac{\tau_{zx}}{G}, \end{cases} \tag{11}$$

Where G is the shear elastic modulus:

$$G = \frac{E}{2(1+\mu)} \tag{12}$$

3. RESULTS AND DISCUSSION

First, the deformed geometrical model was obtained using ANSYS mechanical analysis; then CFD computation based on the deformed geometry was employed to obtain the distribution of fluid flow, species and cell performance. The computation parameters and basic operating conditions used in this research are listed in Table 1 and Table 2.

Table 1. Physical parameters and base conditions [6]

Quantity	Value	Quantity	Value
Operating temperature /K	353.15	Pressure of anode inlet /kPa	1×101.3
Length of the channel /cm	5.0	Pressure of cathode inlet /kPa	1×101.3
Channel width /cm	0.15	Exchange current density of anode /A.m^{-2}	100
Width of plate out channel /cm	0.1	Exchange current density of cathode /A.m^{-2}	1000
Channel thickness /cm	0.1	Mass fraction at cathode inlet O_2	0.21
Shoulder width /cm	0.1	Mass flow rate at the anode inlet /Kg.s^{-1}	5×10^{-6}
Diffusion layer thickness /cm	0.028	Mass flow rate at the cathode inlet /Kg.s^{-1}	6×10^{-7}
Catalyst layer thickness /cm	0.001	Mass fraction at anode inlet H_2	0.8
Membrane thickness /cm	0.005	Mass fraction at cathode inlet H_2O	0.2

Table 2. PEMFC electrochemical and physical parameters

Components / Parameters	Bipolar plate	Gas diffusion layer	Catalyst layer	membrane
Modulus of elasticity (MPa)	13000	5.54	249	232
Poisson's ratio	0.26	0.256	0.3	0.253
Original porosity	0	0.78	0.3	-
Specific heat ($J \cdot kg^{-1} \cdot K^{-1}$)	1580	700	3300	4000
Heat conduction coefficient ($W \cdot m^{-1} \cdot K^{-1}$)	150	25	1	0.95
Electric conductivity ($S \cdot m^{-1}$)	20000	300	300	9.825

3.1 Displacement and strain under different loading forces

Figure 2 plots the total deformation under different assembly pressures of 0.5, 1.0, 1.5, 2.0, 2.5 and 3.0 MPa respectively. The black frame indicates the original position before compression. Because the bipolar plates have a greater modulus of elasticity than do the porous media of the GDL and MEA, and the modulus of elasticity of the GDL is much less than that of the MEA, the deformation will mainly occur in the GDL. The deformation of the MEA can be neglected in the range of pressures studied. It can be seen from the figure that total geometrical deformation increases with increasing assembly pressure. Deformation of the GDL increases too, maximum deformation occurring under the ribs. The deformation of the GDL is about 0.043 mm or 15% of original thickness for an assembly pressure of 0.5 MPa; about 0.087 mm or 31% of original thickness for an assembly pressure of 1.0 MPa; the deformation of the GDL will be over 60% of original thickness for an assembly pressure of 2.0 MPa; the deformation of the GDL will be almost 93% of the original thickness for an assembly pressure of 3.0 MPa. It is over-compressed already. The GDL deformation will reduce the effective diffusion area and the porosity of the porous media.

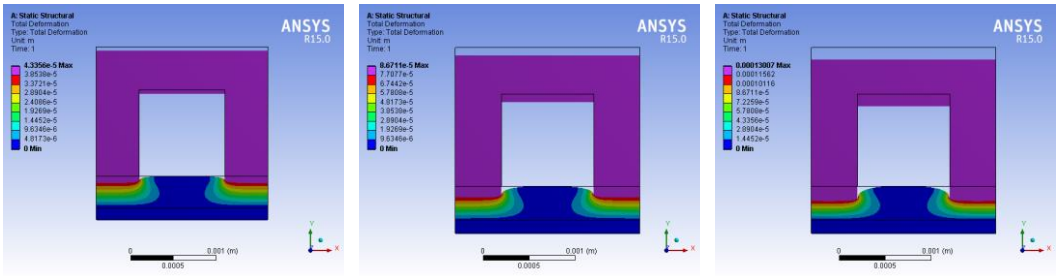

a 0.5 MPa b 1.0 MPa c 1.5 MPa

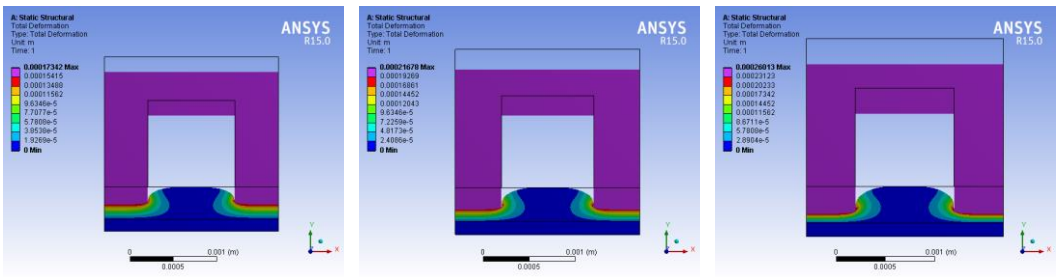

d 2.0 MPa e 2.5 MPa f 3.0 MPa

Figure 2. Total deformation of PEMFC anode under different pressures

The deformed geometry under different assembly pressures is shown in figure 3 where it can be seen that the GDL part under the ribs is obviously deformed, increasing as assembly pressure increases. Deformation of the GDL will reach about 50% under an assembly pressure of 2.0 MPa. However, the part under the channel will have zero deformation. This means that after compression the GDL will intrude into the channel.

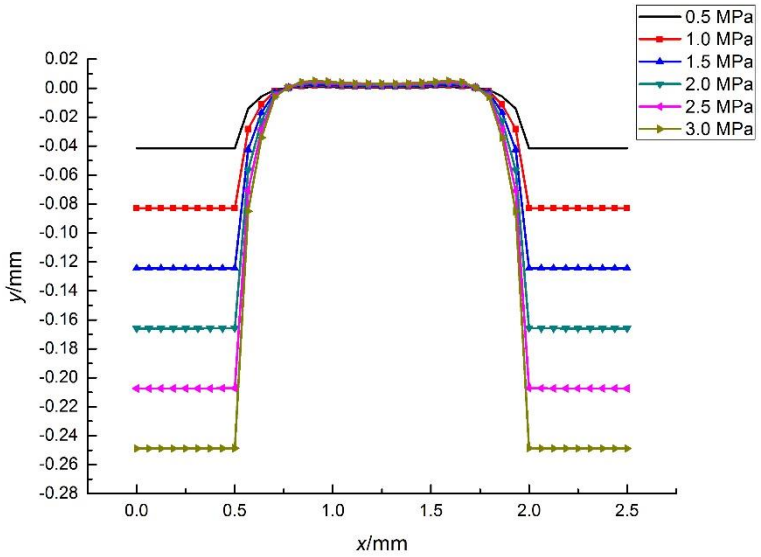

Figure 3. GDL deformation under different assembly pressures

The geometrical model for CFD software FLUENT was reconstructed by AUTOCAD based on the deformation geometry under compression. After reconstruction, the geometry obtained was imported into Gambit and meshed as shown in figure 4. The geometry model was meshed about 0.57 million hexahedron grids.

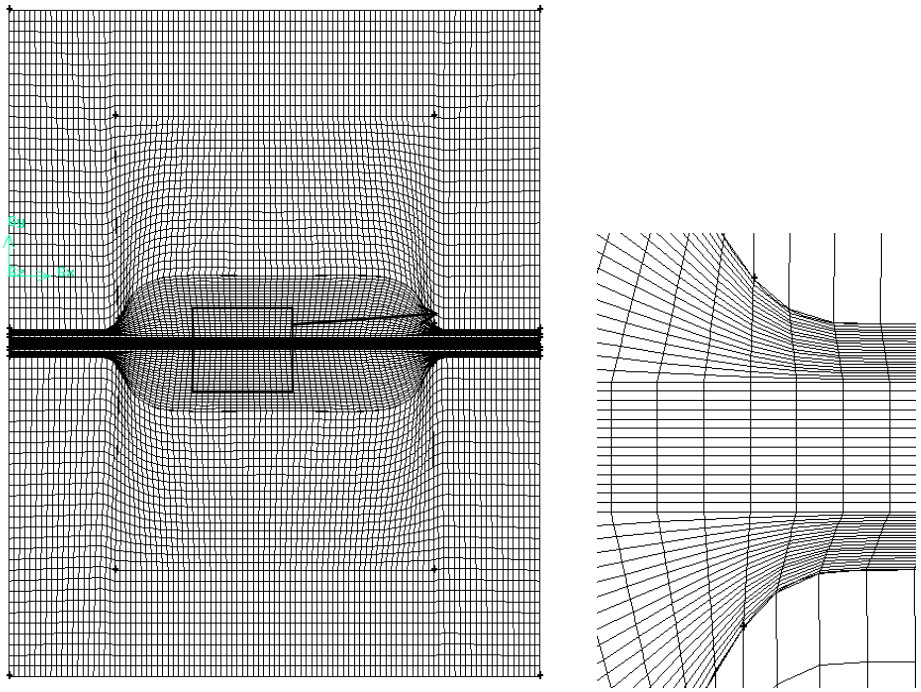

Figure 4. Meshes of deformation geometry model and partial enlarged view

3.2 Effect of assembly pressure on contact resistance

Fuel cell electric resistance includes component internal resistance and contact resistance at the interface, the latter being affected by assembly pressure. Zhou et al. [21] obtained an empirical equation of contact electrical resistance for the interface between the GDL and the carbon bipolar plate. When the material of the GDL is TGP-H carbon paper, and the bipolar plate material is TB-8, the equation is written as follows:

$$R_c = 2.2163 + \frac{3.5306}{p_c} m\Omega cm^{-2} \tag{13}$$

$$p_{assembly} \cdot A_{assembly} = p_c \cdot A_c \tag{14}$$

Where R_c is contact resistance, p_c is contact pressure (MPa), $p_{assembly}$ is assembly pressure, $A_{assembly}$ is the area on which the assembly pressure acts as.

It can be seen from Figure 5 that contact resistance decreases as the assembly pressure increases. As the assembly pressure reaches 0.5-1.0 MPa, the contact resistance decreases rapidly. The contact resistance is 5.04 $m\Omega.cm^{-2}$ for an assembly pressure 0.5 MPa. However it will decrease to 3.63 $m\Omega.cm^{2}$, a drop of 39%, as the assembly pressure increases to 1.0 MPa. Above an assembly pressure of 2.0 MPa, the contact resistance decreases more slowly as assembly pressure increase. This implies that good contact has been achieved at about 2.0 Mpa. Any further increase of assembly pressure may damage the GDL [22].

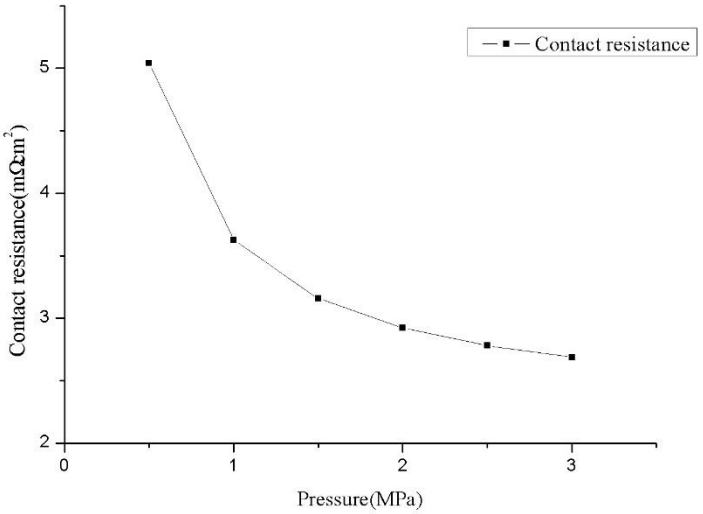

Figure 5. Contact resistance varies with assembly pressure

3.3 Effect of assembly pressure on the species transportation

Figure 6 illustrates the O_2 concentration distribution under different assembly pressures, the gas flowing from left to right. It can be seen that concentrations decrease in the flow direction because of reactant consumption in the catalyst layer (CL). The concentration around the inlet does not change obviously for the enough provision.

When the assembly pressure is small (0.5-1.0 MPa), the porosity and permeability are little affected. The oxygen concentration decreases along the flow direction in the second half section. As the assembly pressure increases to 1.5-3.0 MPa, the oxygen concentration decreases at the end of channel for the decrease of transportation performance as the decrease of porosity and permeability. Thus the effect of assembly pressure on transportation performance cannot be neglected, especially at higher values. The decrease in transportation performance reduces the reaction rate of reactant species and so impairs cell performance.

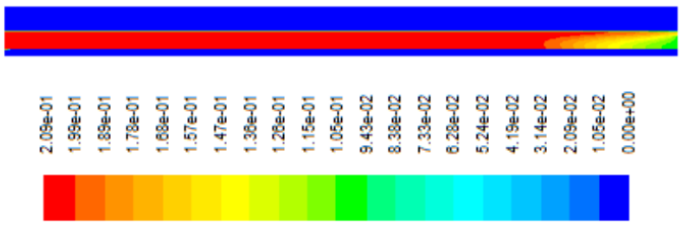

a 0.0 MPa (No compression)

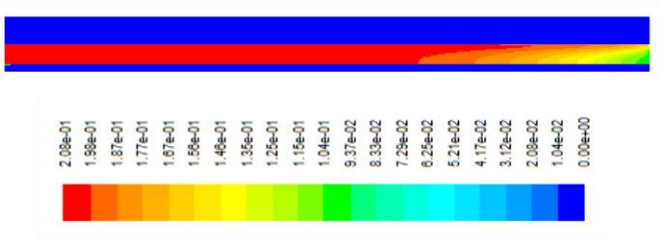

b 0.5 MPa

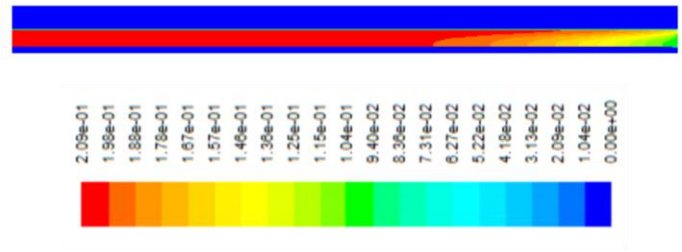

c 1.0 MPa

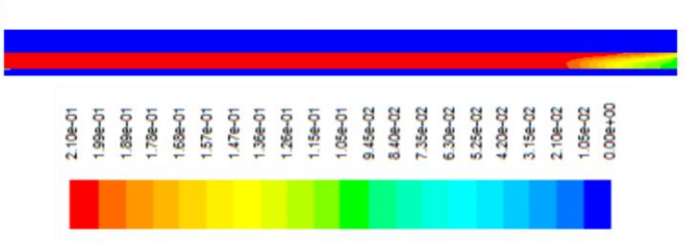

d 1.5 MPa

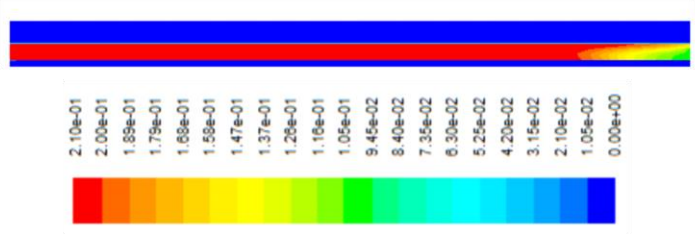

e 2.0 MPa

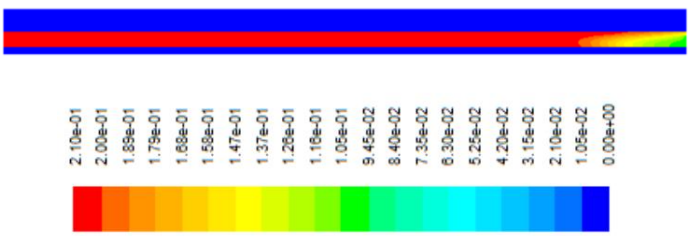

f 2.5 MPa

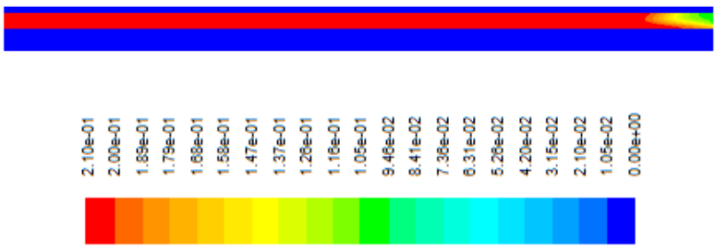

g 3.0 MPa

Figure 6. O_2 concentration in the middle of the *yz* plane under different assembly pressures

3.4 Effect of assembly pressure on cell performance

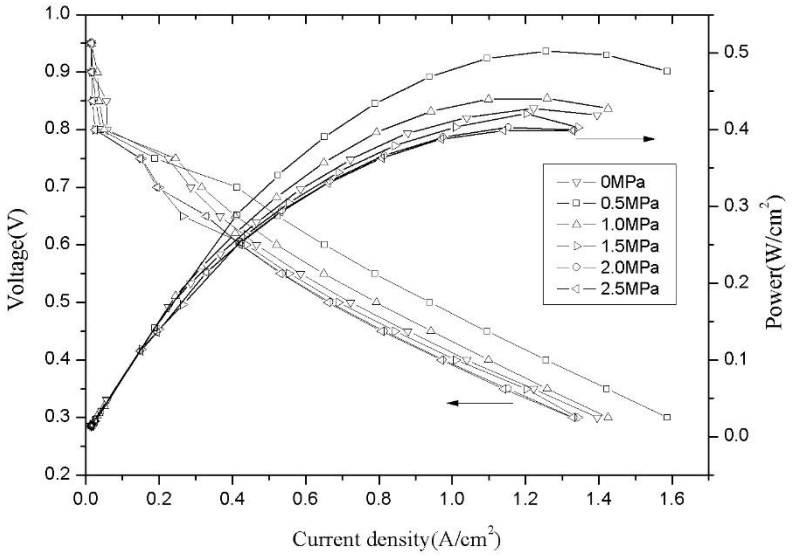

Figure 7. Effect of assembly pressures on output power

Figure 7 plots the polarization performance under different assembly pressures. It can be seen that the cell performance under assembly pressures of 0.5-1.0 MPa is better than for other assembly pressures. At first, contact resistance will decrease with increasing assembly pressure. This will increase the output current for the same voltage; however both porosity and permeability will decrease as assembly pressure increases. This will reduce the reactant species transportation and reaction rate and the corresponding cell performance. Thus, the fuel cell will perform best under an assembly pressure of 0.5-1.0 MPa, which agrees with the literature [13]. Furthermore, the operating conditions used in this research are very similar to the experimental conditions of Lee [23] and Zhou [14, 15], which means the computed results are reliable.

4. CONCLUSIONS

The PEMFC deformation and especially the GDL deformation under different assembly pressures were studied in depth using numerical simulation employing solid mechanics software ANSYS. The transportation phenomena inside the fuel cell and corresponding cell performance were computed based on the deformed geometrical model and CFD. The deformed geometry was exported from ANSYS and transferred to the geometry model which can be used by pre-process software Gambit of CFD software FLUENT. The distribution of species concentrations, strains and stresses were obtained. The influence of assembly pressures on fuel cell performance and transportation parameters such as porosity and contact resistance was investigated in this research. Results show that cell performance is best under an assembly pressure of 0.5-1.0 MPa, which agrees well with the literature and experimental data.

ACKNOWLEDGEMENTS
This work was partly sponsored by the Zhejiang Provincial Natural Science Foundation of China (Q16B030003), Academic Exchange Project of Zhejiang Provincial Natural Science Foundation of China (S17A020001) and the China Scholarship Council foundation (201708330014). The authors would like to thank Mr. Brian Grove McLernon for polishing English.

References

1. Z. Niu, K. Jiao, Y. Wang, Q. Du, Y. Yin, *Int. J. Energy Res.,* 42(2018)802.
2. M. Haghayegh, M.H. Eikani, S. Rowshanzamir, *Int. J. Hydrogen Energy*, 42(2017)21944.
3. Q.G. Zhang, L.F. Xu, J.Q. Li, M.G. Ouyang, *Int. J. Hydrogen Energy*, 43(2018)1736.
4. G. Hu, G. Li**,** Y. Zheng, Z. Zhang, Y. Xu, *J. Energy Inst.*, 87(2014)163.
5. G. Hu, J. Fan, *Energy & Fuels*, 20(2006) 738.
6. G. Hu, J. Fan, *J. Power Sources*, 165(2007)171.
7. D.H. Ahmed, H.J. Sung, J. Bae, *Int. J. Hydrogen Energy*, 33(2008)3786.
8. A. Bates, S. Mukherjee, S. Hwang, S.C. Lee, O. Kwon, G.H. Choi, S. Park, *Int. J. Hydrogen Energy*, 38 (2013)6481.
9. X. Xing, K. Lum, H. Poh, Y. Wu, *J. Power Sources*, 195(2010)62.
10. W.K. Lee, C.H. Ho, J.W.V. Zee, M. Murphy, *J. Power Sources*, 84(1999)45.
11. T. J. Mason, J. Millichamp, T. P. Neville, A. El-kharouf, B. G. Pollet, D.J.L. Brett, *J. Power Sources*, 219(2012)52.
12. S. Yim，B. Kim, Y. Sohn, Y. Yoon, G. Park, W. Lee, C. Kim, Y. Kim, *Current Applied Physics*, 10(2010)S59.
13. I. Taymaz, M. Benli, *Energy*, 35(2010)2134.
14. Y. Zhou, G. Lin, A. J. Shih, S. J. Hu, *J. Power Sources*, 163(2007)777.
15. Y. Zhou, G. Lin, A.J. Shih, S.J. Hu, *ASME J. Fuel Cell Science and Technology*, 6(2009)0410051.
16. Y. Zhou, G. Lin, A.J. Shih, S.J. Hu, *J. Power Sources*, 192(2009)544.
17. K. Oh, P. Chippar, H. Ju, *Int. J. of Hydrogen Energy*, 39(2014)2785.
18. P. Chippar, K. Oh, D. Kim, T. Hong, W. Kim, H. Ju, *Int. J. of hydrogen energy*, 38(2013)7715.
19. T. G. Tranter, A. D. Burns, D.B. Ingham, M. Pourkashanian, *Int. J. Hydrogen Energy*, 40(2015)652.
20. G. Hu , X. Wu , Y. Suo , Y. Xia, Y. Xu, Z. Zhang, *Int. J. Electrochem. Sci.*,13(2018)2080.
21. P. Zhou, C. W. Wu, G. J. Ma, *J. Power Sources*, 163(2007)874.
22. L. H. Zhang, Y. Liu, H. Song, S. Wang, Y. Zhou, S.J. Hu, *J. Power Sources*, 162(2016)1165.

23. S. J. Lee, C. D. Hsu, C. H. Huang, *J. Power Sources,* 145(2005)353.